

Influence of pH on the Micelle-to-Vesicle Transition in Aqueous Mixtures of Sodium Dodecyl Benzenesulfonate with Histidine

Yamaira I. González,[†] Hisanori Nakanishi,[‡] Maria Stjerndahl,[§] and Eric W. Kaler^{*,†}

Center for Molecular Engineering and Thermodynamics, University of Delaware, Newark, Delaware 19716, Faculty of Science and Technology, Tokyo University of Science, 2641 Yamazaki, Noda, Chiba 278-8510, Japan, and Department of Materials and Surface Chemistry, Chalmers University of Technology, Göteborg, Sweden

Received: January 7, 2005; In Final Form: April 3, 2005

Small unilamellar vesicles (~100 nm in diameter) form spontaneously in aqueous mixtures of histidine and sodium dodecyl benzenesulfonate. By manipulating pH, a gradual transition from micelles to vesicles to bilayers to precipitate is observed. The self-assembly of vesicles occurs over a wide range of compositions when the solution pH is lower than 6.0, the pK_a of the imidazole moiety on the histidine molecule. This phenomenon is likely the result of attractive interactions between the negatively charged benzenesulfonate headgroups and the positively charged imidazole group in the amino acid. Similar results are obtained when imidazole salt itself is used.

Introduction

Colloidal assemblies, for example, micelles,^{1–3} vesicles,^{4,5} or fibers,⁶ that are responsive to changes in surrounding conditions such as pH, temperature, or UV light could be potentially used as templates for materials synthesis^{7–9} or drug carriers and delivery devices.^{10–12} Of particular interest are pH-sensitive vesicles, whose closed bilayer structure allows for the encapsulation and targeted release of molecules. Hence, depending on the application, efforts have been directed toward the formulation of vesicles that reversibly form or disrupt at a certain pH. For example, in mixtures of ionizable lipids or anionic and neutral lipids, the onset of instability of a lamellar phase with respect to an inverted hexagonal phase can be tuned to occur at a pH value that depends on the liposome composition.¹³

Custom-made amphiphiles such as amino acid amphiphiles,¹⁴ gemini surfactants,^{15,16} and bolaamphiphiles¹⁷ that carry specific ionizable carboxyl and amine groups offer an alternate and novel way for the formation of pH-sensitive assemblies and perhaps vesicles. By changing pH, the degree of ionization of these groups is changed, and consequently, the surfactant area per headgroup and the molecular packing parameter are modified. Thus, by changing pH, vesicles can form for certain degrees of protonation (α).^{16,18} Interestingly, when the headgroup is chiral, fibers are often obtained.^{17,19}

Vesicles can also form and undergo structural transitions upon the partial protonation of marine-based lipid mixtures,²⁰ fatty acids such as oleic acid,²¹ or mixtures of fatty acids or diacylsuccinylglycerols with phosphatidylethanolamine.²² Similarly, protonation of oleyldimethylamine oxide induces a reversible change from threadlike micelles to vesicles at the half-protonated state ($\alpha = 0.5$).²³ At $\alpha = 0.5$, vesicles also form spontaneously from the addition of sodium 2-naphthalene-sulfonate (Na^+NphS^-) to micellar solutions of tetradecyldim-

ethylamine oxide $\cdot\frac{1}{2}HCl$.²⁴ This is in contrast to the case of the fully ionized amine oxide ($\alpha = 1$) where lamellar droplets form instead of vesicles.²⁵ The combined effect of the ionization degree and the strong binding of the $NphS^-$ counterion leads to the formation of vesicles rather than the usual lamellar liquid crystalline phase.

Binding of hydrotrope and the degree of protonation of ionizable groups are both crucial in promoting the spontaneous self-assembly of vesicles upon the addition of the water-soluble initiator 2,2'-azobis[2-(2-imidazolin-2-yl)propane] dihydrochloride (V-44) to micellar solutions of sodium dodecyl benzenesulfonate (SDBS).²⁶ With a lowering of pH, the imidazolium end groups on the initiator protonate and bind to the SDBS headgroup, thus driving a micelle-to-vesicle transition.

Here, the phase behavior particularly with respect to micelle-to-vesicle transitions of mixtures of SDBS with the amino acid histidine is investigated. It is attractive to use amino acids as additives to surfactant systems that could have potential biochemical applications. Unlike V-44, histidine is a stable and soluble molecule in water, which allows for a systematic study of the effect of pH. Finally, the self-assembly of vesicles in mixtures of imidazole with SDBS is investigated and compared to that observed in mixtures of histidine with SDBS. The simplicity of preparation, the stability of the vesicles, and the availability of other amino acids are promising for future studies of surfactant–amino acid assemblies as pH-dependent carriers of compounds.

Materials and Methods

Materials. Hard-type (branched-chain)²⁷ SDBS was purchased from TCI America. L-Histidine monohydrochloride monohydrate (His-HCl), L-histidine, and imidazole were obtained from Sigma. Hydrochloric acid (1 N) was purchased from Acros Organics. All chemicals were used as received.

Sample Preparation. Stock solutions of SDBS, His-HCl, histidine, imidazole, and HCl were prepared in deionized water (Milli-Q) or D_2O (Cambridge Isotopes) and mixed at room temperature at the desired molar fraction of each component.

* To whom correspondence should be addressed. Phone: 1(302) 831-3553. Fax: 1(302) 831-6751. E-mail: kaler@che.udel.edu.

[†] University of Delaware.

[‡] Tokyo University of Science.

[§] Chalmers University of Technology.

All the solution mixtures were gently shaken until a uniform-colored, one-phase solution was observed. The solutions were not subjected to any type of mechanical agitation. pH measurements were performed at room temperature using an Orion 420A pH meter and a Cole Parmer BNC glass electrode after equilibrating the solutions for 12 h. Samples were examined visually to determine the number of phases. Phase boundaries were assigned after the visual appearance of the samples remained unchanged with time. The phase behavior of mixtures at 25 °C is depicted using a pseudoternary phase representation. Provisionally, transparent solutions were identified as micellar, while isotropic bluish solutions suggested the presence of vesicles. For light scattering measurements, solution mixtures were filtered through 0.45 μm PTFE filters and flame-sealed in 1 mL ampules. All samples were then kept during the equilibration and characterization studies in a thermostated bath at 25 °C.

Surface Tension. Surface tension was measured at 25 °C using a K10T digital tensiometer (Krüss) with a Wilhelmy plate. Equilibrium was confirmed by multiple measurements of a constant surface tension, and at least three measurements were taken for each point.

Quasielastic Light Scattering (QLS). Measurements of the aggregate average hydrodynamic size were made at 25 °C using a Brookhaven BI-200SM goniometer, a BI-9000AT correlator, and a Lexel 300 mW Ar ion laser ($\lambda = 488$ nm) at a scattering angle of 90°. Intensity correlation data were analyzed by the method of cumulants²⁸ to provide the average decay rate, $\langle\Gamma\rangle = q^2D$, where D is the apparent diffusion coefficient, and the normalized variance, $\nu = (\langle\Gamma^2\rangle - \langle\Gamma\rangle^2)/\langle\Gamma\rangle^2$, which is a measure of the width of the distribution of the decay rates. Stokes' law was used to calculate the apparent hydrodynamic radii from the measured diffusion coefficients. CONTIN analysis was also used to quantify the distribution of aggregates.²⁹

Cryogenic Transmission Electron Microscopy (cryo-TEM). Specimens for cryo-TEM were prepared in a controlled environment vitrification system (CEVS) described in detail by Bellare et al.³⁰ The samples were equilibrated inside the chamber at 25 °C and a relative humidity of 95–99%. A drop of the solution was placed on a lacey carbon film, supported by a copper grid (Ted Pella, Redding, CA), and thin liquid films of 50–500 nm cross sections were then formed by gently blotting away excess liquid on the grid with a piece of filter paper. The liquid films were then vitrified by plunging the grid into liquid ethane, held at -180 °C by a surrounding thermostated pool of liquid nitrogen. The grid was transferred under liquid nitrogen onto the tip of a Gatan model 626 cold stage. The specimens were maintained at below -168 °C and were examined by a JEOL 2000 FX transmission electron microscope operated at 100 kV. Images were recorded using a Multiscan Gatan CCD camera at low dose.

Small-Angle Neutron Scattering (SANS). Neutron scattering experiments were performed on the NG7 30m spectrometer at the National Institute of Standards and Technology (NIST) in Gaithersburg, MD. Neutrons of wavelength $\lambda = 6$ Å with a spread of 11% were incident on quartz “banjo” cells with 2 mm path lengths. Three different sample-to-detector distances of 13.7, 4, and 1 m were used to cover an overall scattering vector (q) range of 0.003–0.53 Å⁻¹. The data were corrected for detector efficiency, background scattering, empty cell scattering, and sample transmission and placed on an absolute scale using NIST protocols and calibration standards. For the data analysis, the ideal model scattering curves were smeared

to take into account corrections due to the instrument resolution.³¹ The quality of the fit was assessed from the reduced χ^2 values.

SANS Analysis. The SANS scattering curves of samples containing vesicles were fitted using a polydisperse core–shell model, where the vesicles are assumed to have a polydisperse core with constant shell thickness (t) and any intervesicle interactions are neglected.³² In this case, for a polydisperse system of unilamellar noninteracting vesicles, the scattered intensity as a function of the scattering vector is given by

$$I(q) = \frac{d\Sigma}{d\Omega}(q) = n \int_0^\infty G(r_c) P^2(qr_c) dr_c \quad (1)$$

where n is the number density of vesicles, $P(qr_c)$ is the form factor of a single particle (e.g., vesicles) consisting of a core and an outer shell, and $G(r_c)$ is the normalized probability of finding a particle with a core radius between r_c and $r_c + dr_c$. $G(r_c)$ is modeled as a Schulz distribution, so

$$G(r_c) = \frac{r_c^Z}{\Gamma(Z+1)} \left(\frac{Z+1}{\bar{r}_c} \right)^{Z+1} \exp\left(-\frac{r_c}{\bar{r}_c} (Z+1) \right) \quad (2)$$

where \bar{r}_c is the mean core radius and Z is related to the variance (σ^2) of the core radius by

$$\frac{1}{Z+1} = \frac{\sigma^2}{\bar{r}_c^2} \quad (3)$$

The form factor is

$$P(qr_c) = \frac{4\pi}{q^3} (\rho_b - \rho_c) \{ J_1(qr_c + qt) - J_1(qr_c) \} \quad (4)$$

where $J_1(x) = \sin(x) - x \cos(x)$ and ρ_b and ρ_c are respectively the scattering length densities (SLDs) of the bilayer and the core (taken as the solvent D₂O).

The SLDs were calculated by adding the scattering amplitudes of each group or atom in a molecule and dividing the total by the corresponding molecular volume. The SLD of D₂O is 6.3×10^{-6} Å⁻², and the SLD of the bilayers was calculated assuming the bilayer is made of an equimolar composition of the oppositely charged components. This assumption has little influence on the results.

Spectra from samples containing micelles were fitted to a model incorporating an ellipsoidal or cylindrical form factor. The Hayter and Penfold rescaled mean spherical approximation and the Yukawa form of the potential between the micellar “macroions” were used to account for interparticle interactions in terms of a structure factor $S(q)$.³³ The intensity model for monodisperse, interacting ellipsoidal micelles is

$$I(q) = \frac{d\Sigma}{d\Omega}(q) = n \int_0^1 |F(q,\mu)|^2 d\mu \left(1 + \frac{\langle F(q,\mu) \rangle^2}{\langle |F(q,\mu)|^2 \rangle} (S(q) - 1) \right) \quad (5)$$

with

$$F(q,\mu) = v(\rho_m - \rho_s) \frac{3j_1(x)}{x} \quad (6)$$

and

$$x = q[a^2\mu^2 + b^2(1 - \mu^2)]^{0.5} \quad (7)$$

TABLE 1: Results from Fitting an Ellipsoidal Model, a Cylindrical Model, or the Smeared Polydisperse Core–Shell Model to SANS Spectra from Samples Containing Micelles or Vesicles at Various SDBS, Histidine, and HCl Compositions^a

[SDBS] (mM)	[His] (mM)	[HCl] (mM)	model	outer diameter (nm)	bilayer thickness (nm)	polydispersity	$\sqrt{\chi^2/N}$	
19	26	26	core–shell (Figure 3)	92 ± 1	2.3	0.14 ± 0.1	5.6	
[SDBS] (mM)	[His] (mM)	[HCl] (mM)	model	length (nm)	radius (nm)	charge	effective salt concn (mM)	$\sqrt{\chi^2/N}$
19	1.4	1.4	ellipsoidal (Figure 3)	4.8 ± 0.2	1.6	−17 ± 1	7	1.2
30	50	0	cylindrical (Figure 8)	3.7 ± 0.1	1.5	−22 ± 4	9	1.6
30	50	20	cylindrical (Figure 8)	9.6 ± 0.3	1.6	−18 ± 2	2.6	1.8

^a In the micellar samples, the Hayter and Penfold rescaled mean spherical approximation was used for the structure factor. The quality of the fits is assessed from the reduced χ^2 error between model and data.

where a is the semimajor axis of the micelle, b is the semiminor axis, $j_1(x)$ is the first-order spherical Bessel function, μ is the cosine of the angle between the directions of a and q , v is the volume of the micelles, and ρ_m and ρ_s are the coherent scattering length densities of the micelle and the solvent, respectively. The adjustable parameters were a , b , and the net charge of the surfactant–amino acid micelles.

Likewise, the intensity model for monodisperse rigid circular cylinders is³⁴

$$I(q) = \frac{d\Sigma}{d\Omega}(q) = n \int_0^{\pi/2} |F(q, \alpha)|^2 d \sin \alpha d \alpha \left(1 + \frac{\langle F(q, \alpha) \rangle^2}{\langle |F(q, \alpha)|^2 \rangle} (S(q) - 1) \right) \quad (8)$$

with

$$F(q) = v(\rho_m - \rho_s) \frac{\sin\left(\frac{L}{2} q \cos \alpha\right) 2j_1(qr \sin \alpha)}{\frac{L}{2} q \cos \alpha qr \sin \alpha} \quad (9)$$

Here, α is the angle between the cylinder axis and the scattering vector (q), r is the cross-sectional radius, and L is the length of the micelle. The adjustable parameters were r , L , and the net charge of the surfactant–amino acid micelles.

For model calculations, 20% of the micelle amphiphiles were initially assumed to disassociate and the ionic strength was set equal to the sum of the concentration of unassociated surfactant molecules at the critical aggregation concentration and the concentration of chlorine ions in solution. Histidine molecules bearing the cationic form of the imidazole group were assumed to be bound to SDBS, while histidine zwitterions were not taken into account when setting the ionic strength. The final value of the salt concentration used to calculate the micelle charge is listed in Table 1. The fitted parameters minimized the value of χ^2 for the model fit of each SANS spectrum.

Results

Micelle Formation. The surface activity and critical micelle concentration (cmc) of aqueous mixtures of SDBS with histidine were investigated using tensiometry. The cmc of pure SDBS is 3.0 mM. Histidine does not form aggregates and is slightly surface active with a surface tension of 70 mN/m at its solubility limit of 250 mM at 20 °C. On the other hand, the solubility of equimolar His-HCl at 20 °C is 1.1 M and its surface tension is 40 mN/m. The benefit of adding His-HCl to SDBS solutions is illustrated by the lower critical aggregation concentration (cac) of the mixtures: 2.5 mM for $\delta = 0.8$ and 1.0 mM for $\delta = 0.2$, where $\delta = \text{moles of SDBS}/(\text{moles of SDBS} + \text{moles of His-HCl})$. Likewise, an increased surface activity for the mixture is

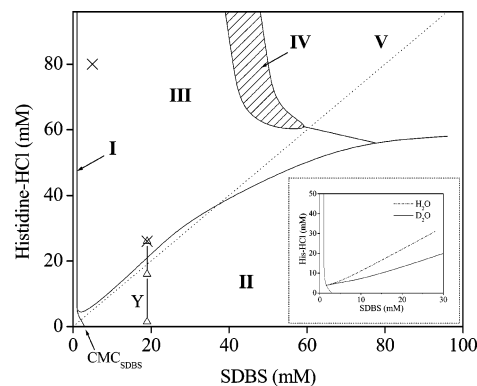


Figure 1. Water-rich corner of the pseudoternary phase diagram of SDBS, histidine-HCl–H₂O (His-HCl), and H₂O at 25 °C. The phase regions are the following: (I) monomeric species, (II) micelles, (III) vesicles, (IV) multiple phases, and (V) precipitate. The dotted line represents equimolar compositions of SDBS and amino acid. The shaded area designates a transition region from vesicles to precipitate in which several phases with different degrees of turbidity and an additional oily phase at the bottom of the sample coexist. The inset shows the shift of the phase boundary between the micellar and the vesicular region when D₂O is used as the solvent. The vertical line (Y) represents samples made at a constant concentration of SDBS (19 mM) and an increasing amount of His-HCl. These samples were characterized by SANS (Figure 3).

evident when comparing the surface tension at the cmc of the pure surfactant (31 mN/m) with the corresponding values obtained at the cac of the mixtures: 28 mN/m ($\delta = 0.8$) and 27 mN/m ($\delta = 0.2$). Beyond the cac, the monomers in solution self-assemble into micelles.

Phase Diagram. The water-rich corner of the pseudoternary phase map (Figure 1) of mixtures of SDBS, His-HCl (the equimolar mixture of His and HCl), and H₂O at 25 °C is the result of observations after 6 months of equilibration. Along the binary axis of His-HCl–H₂O (region I), solutions are transparent at all His-HCl concentrations studied. From QLS, there is no evidence of microstructure formation in this region. Solutions also appear transparent along the SDBS–H₂O axis for low to intermediate concentrations of histidine (region II). Throughout this regime, QLS and SANS measurements confirm the presence of micelles and a gradual transition from micelles to vesicles with increasing concentration of His-HCl.

Above the equimolar line and for SDBS concentrations below approximately 40 mM, bluish isotropic solutions coexist with a small “wisp” of precipitate (region III). This wisp is also seen in micellar samples near the vesicle–micelle phase boundary. Here, the presence of vesicles is confirmed by QLS, cryo-TEM, and SANS. At higher SDBS concentrations, a clear supernatant phase coexisting with a noticeable opaque white precipitate phase (region V) is obtained. Between these two regions, the mixtures phase-separate (region IV) into several

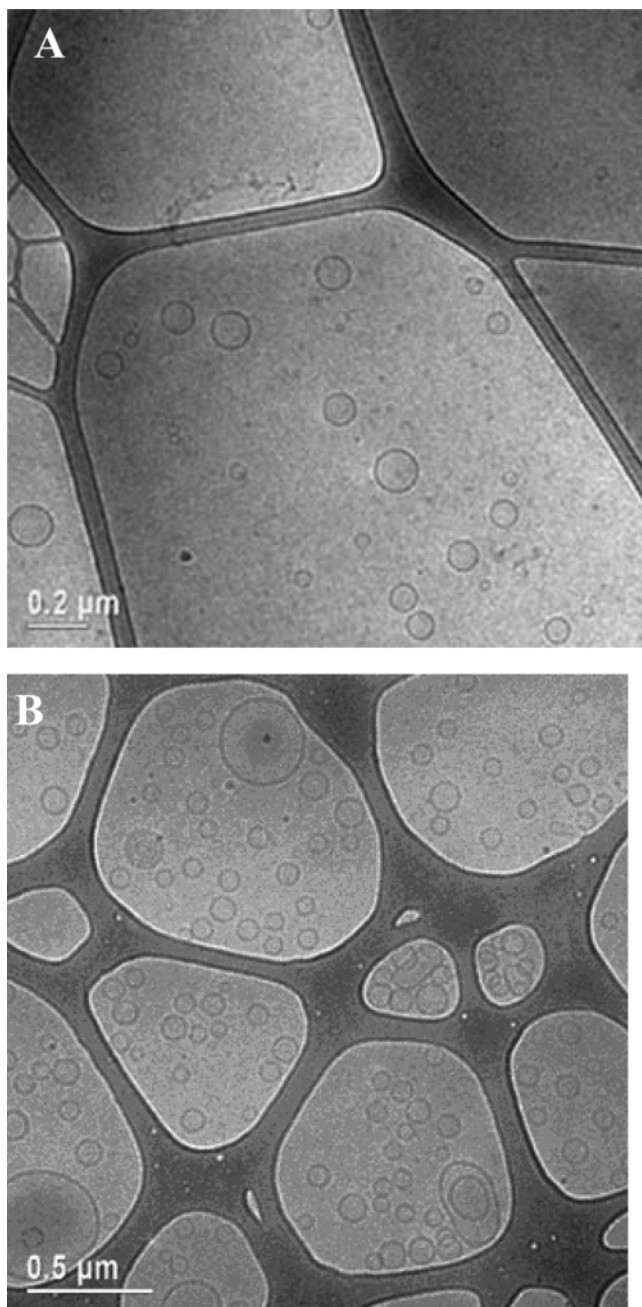


Figure 2. Cryo-TEM micrographs after the sample has aged for 5 weeks for (A) a 5 mM SDBS and 80 mM histidine-HCl mixture in H₂O showing mostly unilamellar vesicles (the smaller vesicles have a diameter of about 30 nm, and the larger vesicles have a diameter of about 100 nm) and (B) a 19 mM SDBS and 26 mM histidine mixture in D₂O showing mostly unilamellar vesicles (the smaller vesicles have a diameter of 80–150 nm, and a few larger vesicles have a diameter of 200–300 nm).

phases with different degrees of turbidity and an additional oily phase at the bottom of the sample. Region IV was not characterized in detail.

a. Effect of D₂O. The inset in Figure 1 shows the downward shift of the phase boundary between the micellar and the vesicular region when H₂O is replaced with D₂O. Similar changes occur in other catanionic mixtures³⁵ and are due to stronger hydrogen bonds in the deuterated solvent.³⁶ D₂O favors the formation of large aggregates, and here, there is a significant shift for the SDBS–His-HCl mixtures.

b. Vesicle Microstructures. The cryo-TEM micrographs in Figure 2 are representative of the vesicle microstructures found

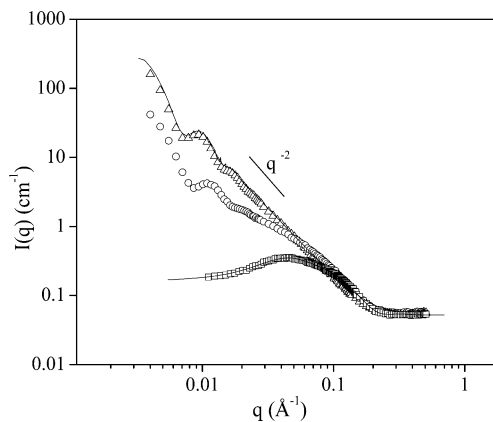


Figure 3. SANS results for mixtures of 19 mM SDBS and varying concentrations of His-HCl: (Δ) 26 mM; (\circ) 16 mM; (\square) 1.4 mM. The background scattering is not subtracted to show the overlap at high q values. The q^{-2} slope for the 26 mM His-HCl sample is a signature of vesicles, while the 1.4 mM sample exhibits a scattering typical of micelles. The scattering of the 16 mM appears to be that of a mixed population of vesicles and micelles.

in region III (\times symbols in Figure 1) after aging for 5 weeks. Figure 2A corresponds to an aqueous sample with a low SDBS concentration of 5 mM and a very high His-HCl concentration of 80 mM. On the other hand, the vesicles in Figure 2B are observed in a deuterated solution of 19 mM SDBS and 26 mM His-HCl. A polydisperse population of spherical unilamellar vesicles is found in both cases, although a few elongated and multilamellar vesicles are also seen. The number of vesicles appears higher for the deuterated sample than for the aqueous mixture. This is expected since a lower concentration of 5 mM SDBS in the aqueous sample limits the number of aggregates that can be formed. QLS measurements of these samples yield a z -averaged hydrodynamic diameter of 114 nm.

c. Micelle-to-Vesicle Transition. SANS measurements for samples made at 19 mM SDBS with increasing concentrations of His-HCl provide evidence of a micelle-to-vesicle transition (Figure 3). At 1.4 mM His-HCl, the scattering profile is typical of those for small micelles. The peak at $q = 0.05 \text{ \AA}^{-1}$ is indicative of strong repulsive intermicellar interactions. At 16 mM His-HCl and 26 mM His-HCl, the enhanced scattering at low q values and the minima at $q = 0.01\text{--}0.02 \text{ \AA}^{-1}$ indicate the presence of vesicles. However, the 16 mM His-HCl spectrum is also consistent with a mixed population of vesicles and micelles. The slope at intermediate q values (to the right of the minimum) approaches q^{-1} , which is the scattering characteristic of elongated micelles or rigid cylindrical structures, and the data at high q values overlap those of the micellar sample. In contrast, the 26 mM His-HCl data display a q^{-2} decay pattern along the entire q region that is a signature of bilayers and membrane structures.

Consistently, the 1.4 mM His-HCl data were fitted using the standard model of an ellipsoidal form factor together with the Hayter and Penfold rescaled mean spherical approximation for the structure factor. The best fit suggests the micelles are prolate objects with a cross-sectional radius of 1.6 nm, a length of 4.8 nm, and a negative charge of 17. The 26 mM His-HCl data were fitted to a smeared polydisperse core–shell model capable of capturing the vesicular architecture. The resulting core radius, bilayer thickness, and polydispersity are 43.9 nm, 2.3 nm, and 0.14, respectively, which correspond to vesicles with a number average diameter of 92 nm and an equivalent z -average diameter of 98 nm.³⁷ These values are in good agreement with the vesicle size of 108 nm measured by QLS. A summary of the fitted parameters for these samples is shown in Table 1.

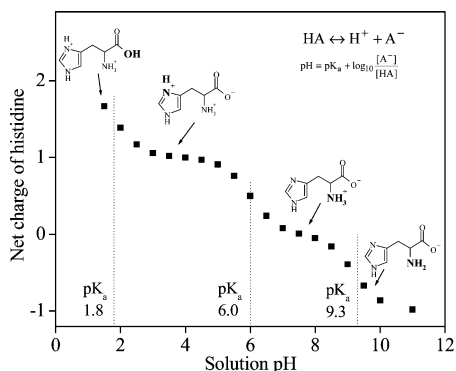


Figure 4. Schematic of the various states of protonation of histidine. The molecule becomes more positively charged at lower pH. The calculation takes into account a species balance and the Henderson–Hasselbalch equation for the weak dissociation of acids.

Effect of pH. The transitions observed above depend on the molar ratio of SDBS to histidine as well as pH. When the amount of His-HCl is increased, the pH is also lowered. Thus, to isolate the effect of these variables on the micelle-to-vesicle transition, the pH was changed for solutions made at a fixed ratio of surfactant and amino acid. The microstructures in several of these solutions were then characterized.

a. Titration of Histidine. Histidine is a weak polyprotic acid with three dissociable hydrogens.³⁸ The pK_a values of these groups, 1.8 (α -COOH), 6.0 (imidazole group), and 9.2 (α -NH₃⁺), are depicted in Figure 4. The degree of dissociation of these groups depends on the pH of the medium, so that a change in pH affects the net charge of the histidine molecules. With a gradual decrease in pH, each of the functional groups of histidine protonate and the molecule becomes more positively charged. The imidazole group is half-protonated when the pH is near 6, and the carboxyl group half-protonates at a pH of about 2.

Sigmoidal curves for the titration of histidine in mixtures with SDBS are shown in Figure 5. The pH range is below a histidine isoelectric point of 7.47; thus, the curves show primarily the titration of the imidazole group. In the absence of SDBS, the curves have a steeper slope than those in which SDBS is present (Figure 5A) and phase separation is not observed regardless of the solution pH. In mixtures with SDBS, pH measurements were done up to about pH 3.2. At a lower pH, the solutions turn milky and precipitate is observed. The normalized curves for each of these mixtures are shown in Figure 5B. Below the equimolar composition of HCl and histidine, the curves almost coincide. Deviations in the slope are clearly observed for a number of equivalents greater than 1. Note that the change of pH with respect to the addition of HCl is more gradual when SDBS is in solution and that the gentlest slope is for the equimolar solutions of histidine with SDBS.

b. QLS Results. Figure 6 shows size distributions obtained from a CONTIN analysis of samples made at a fixed composition of 30 mM SDBS and 50 mM histidine and increasing amount of HCl. Each of these samples is a point on the path **A** (micelles) to **E** (vesicles) represented in the upper left panel. When there is no acid present (Figure 6A), the imidazole group is not protonated. QLS shows a unimodal distribution of micelles of about 2–3 nm, which is the characteristic size range for SDBS micelles. At a lower pH, the distribution shifts toward larger sizes, possibly indicating the presence of elongated micelles (Figure 6B). At pH 5.8, a new population with a size typical of vesicles emerges. The number of aggregates of this size increases as the pH is further lowered and the solution turns

bluish (Figure 6D). Finally, at 50 mM HCl (point **E** in the phase diagram), only one distribution with an average size of 100 nm is obtained. Below pH 3.7, the solutions become more turbid, and at 61 mM HCl (pH 3.2), a milky solution with a large amount of precipitate is observed.

The trend is the same for other ratios of SDBS to histidine (Figure 7). At high pH, the solutions are transparent, indicating the presence of micelles. Lowering the pH eventually causes the solutions to turn bluish, indicating the presence of vesicles, and at a lower pH, precipitate is observed. This micelle-to-vesicle transition also depends on the concentration of histidine for a fixed amount of SDBS. Vesicles form at a lower pH with less histidine in solution, and below 2–3 mM histidine, vesicle formation is not observed regardless of pH. Besides the observed change in color, the presence of vesicles is confirmed by QLS measurements that indicate an average size greater than 60 nm. At the point where the change in color is observed and larger aggregates are measured with QLS, it is likely that both vesicles and micelles are present in solution, as indicated by SANS results.

c. SANS Results. Neutron scattering data for samples of 30 mM SDBS and 50 mM histidine at three different acid concentrations are shown in Figure 8. In the absence of acid, the scattering profile is that of small spheroidal micelles and can be fit well by an ellipsoidal (not shown) or a cylindrical model (Table 1). The peak at $q = 0.05 \text{ \AA}^{-1}$, which is indicative of repulsive interactions, is more pronounced than that for the micelles in Figure 3. The upturn at low values of q is low in intensity, on the order of 0.3 cm^{-1} , and could be the result of a low concentration of larger aggregates, such as what could be found in the wisp observed by eye. At 20 mM HCl, the micelles elongate to about 10 nm, although their cross-sectional radius is preserved. The interaction peak also disappears, indicating that histidine molecules are screening the charge of the micelles. With more acid (35 mM HCl), a different profile is observed at low q values that is indicative of vesicles. The fact that the scattering is somewhere between q^{-2} and q^{-1} and the overlap of this curve with the other micellar curves at high q values both indicate that micelles and vesicles are coexisting in solution. Note the similarity of this curve with that in Figure 3 for 19 mM SDBS and 16 mM His-HCl.

Effect of the Imidazole Moiety. The structure and different conformation states of the imidazole moiety are depicted in Scheme 1. A pH-dependent micelle-to-vesicle transition is also observed in mixtures of SDBS with imidazole (Figure 9). For comparison, the transition in 30 mM SDBS and 50 mM imidazole (circles) is shown against that of histidine at 30 mM SDBS (triangles). With imidazole, the transition occurs at a higher pH than in the case of solutions made with histidine. Also, the minimum amount of imidazole needed to drive vesicle formation is 4 times larger than in the case of histidine.

Discussion

Studies of the effect of pH at different fixed ratios of histidine and SDBS confirm the influential role of pH in driving morphological transitions. The micelle-to-vesicle transition can be explained qualitatively in terms of the net charge of histidine. Lowering the pH to below 6 results in the formation of cationic imidazole moieties that can interact with the negatively charged SDBS headgroups, changing the surface charge density and, therefore, the effective headgroup area. The observed lower cmc and surface tension values for these mixtures are a consequence of the nonideal interactions between these oppositely charged functional groups. If the surface charge density is lowered, the

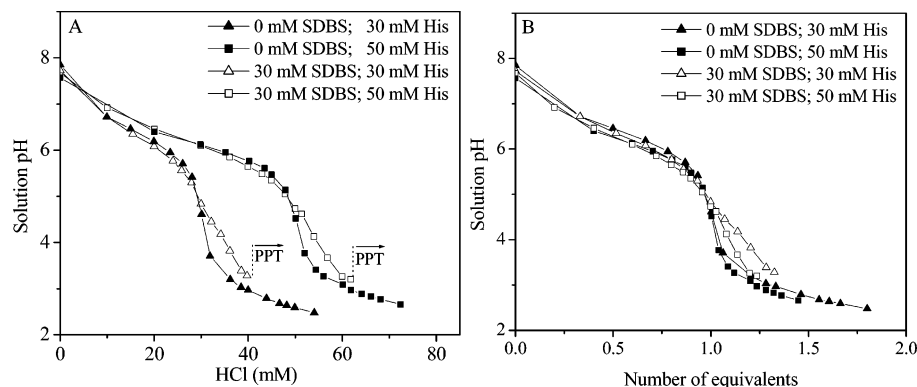


Figure 5. Sigmoidal curves for the titration of histidine in mixtures with and without SDBS. The curves show primarily the titration of the imidazole group: (A) pH as a function of the HCl concentration; (B) pH as a function of the number of equivalents of acid. See text for explanation.

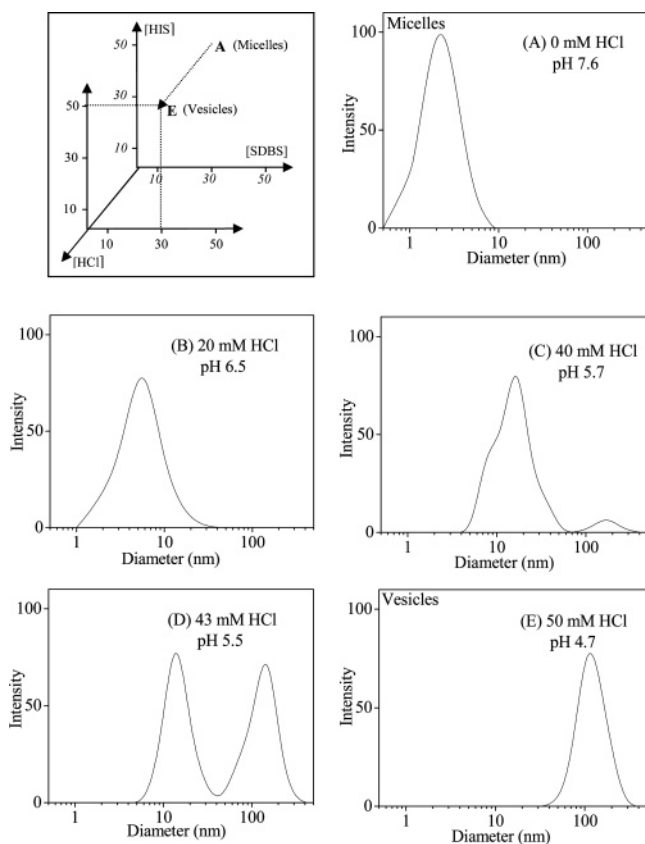


Figure 6. Size distributions obtained from a CONTIN analysis of samples made at a fixed composition of 30 mM SDBS and 50 mM histidine and increasing amounts of HCl. Each of the samples is a point on the path A (micelles) to E (vesicles) represented in the upper left panel. At 0 mM HCl (A), there is a unimodal distribution of micelles of about 2 to 3 nm. With lower pH, the distribution continuously shifts toward larger sizes, suggesting the presence of elongated micelles (B), the coexistence of micelles and vesicles (D), and the presence of vesicles (E).

area per headgroup decreases, and the surfactant packing parameter increases.³⁹ This decreases the net curvature of the surfactant aggregates, so SDBS micelles undergo a structural transition from micelles to rodlike micelles and eventually to aggregates of low curvature such as long wormlike micelles, vesicles, lamellar droplets, or precipitate.

The nature of the species accompanying SDBS can dramatically affect the structural transition and preferred microstructures. Söderman et al.⁴⁰ and Lin et al.⁴¹ observed a direct transition from spherical micelles to vesicles with no threadlike micelle intermediates in mixed solutions of SDBS with the

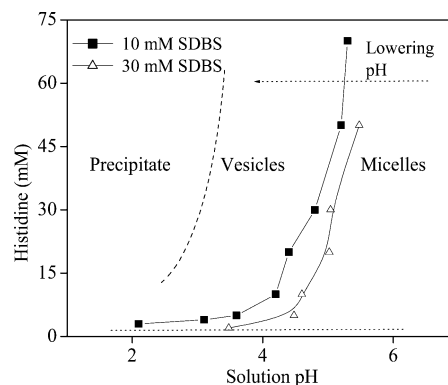


Figure 7. Micelle-to-vesicle transitions in solutions made at different ratios of histidine and SDBS. By lowering the pH, solutions turn bluish, indicating the presence of vesicles. With less histidine in solution, the micelle-to-vesicle transition occurs at a lower pH.

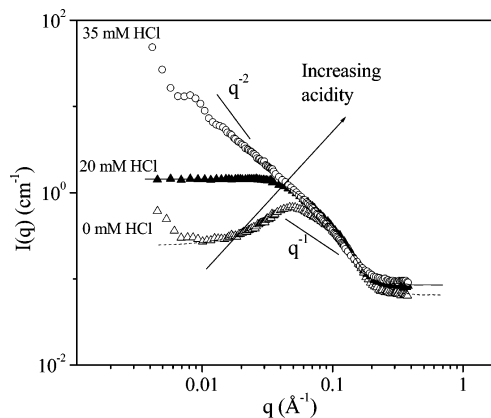


Figure 8. SANS spectra for samples made in D₂O at a fixed molar ratio of 30 mM SDBS and 50 mM histidine and increasing HCl concentration: (Δ) 0 mM HCl; (▲) 20 mM HCl; (○) 35 mM HCl. The background scattering is not subtracted to show the overlap at high q values. The solid lines represent the best fit of the model to the SANS data. Slopes of -1 and -2 are indicated for comparison of the scattering of micelles with that of vesicles.

oppositely charged surfactant dodecyltrimethylammonium chloride or with divalent $\text{Ca}^{2+}/\text{Mg}^{2+}$ ions. On the other hand, Sein et al.⁴² showed that in mixtures of SDBS with NaCl the micelles transform into a phase of flocculated multilamellar aggregates separated from the isotropic electrolyte solution. Fluorescence depolarization measurements indicated an intermediate transition to micelles of elongated geometry. Substitution of NaCl for other alkali chlorides strongly influenced the lyotropic phase behavior of SDBS and the appearance of the resulting lamellar phases.

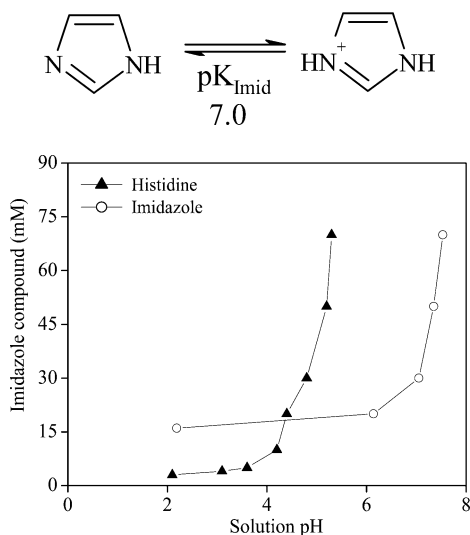
SCHEME 1: Structure of the Imidazole Molecule in Its Free Base (Left) and Protonated (Right) Forms

Figure 9. Micelle-to-vesicle pH-dependent transitions in solutions of 30 mM SDBS and 50 mM imidazole (circles). To the right of the curve, micelles are in solution, while, to the left of the curve, vesicles are observed. For comparison, the transition in 30 mM SDBS and 50 mM histidine (triangles) is also shown.

Here, the sequence of morphological changes is similar to that discussed for mixtures of SDBS with bis(imidazolin) compounds.²⁶ A transition involving micelles, elongated micelles, vesicles, and precipitate takes place with decreasing pH, caused either by increasing His-HCl concentration or by the addition of HCl. This sequence is expected because of the similarity of the imidazolium group in the V-44 analogues and the imidazole side chain in histidine. However, the micelle-to-vesicle transitions in mixtures with histidine are triggered at a lower pH ($\text{pH} < 6$) than the values below nine recorded in solutions with V-44 analogues. The reason for this difference is imidazole has a $\text{p}K_a$ of 6.0, which is substantially lower than values of ~ 10 – 11 for the imidazolium groups.

The transition from spherical micelles to elongated micelles is clear from QLS (Figure 6) and SANS (Figures 3 and 8). Micelle elongation occurs when the pH is decreased but remains above the $\text{p}K_a$ of the imidazole group, so that only a small fraction of the imidazole groups are protonated. The binding of these molecules to the negatively charged benzenesulfonate groups leads to the elongation of the micelles. The effect of binding is reflected by the reduction of the aggregates' net negative charge and the disappearance of the interaction peak. Hassan et al. have characterized by QLS, SANS, NMR, and rheology measurements a similar type of evolution for micellar solutions of sodium dodecyl sulfate upon the addition of the hydrotropic salt *p*-toluidine hydrochloride.^{43,44}

A second transition in which the elongated micelles evolve into vesicles occurs via a region of coexistence of these aggregates. From CONTIN, this transition appears to be continuous so that the number of micelles decreases once vesicles begin to form. The micelles and vesicles do not form separate phases at any point. This is in agreement with numerous reports in which it has been demonstrated by cryo-TEM that elongated micelles and vesicles coexist.^{45–47} An exception to this pattern is the observations of Kawasaki et al.²⁴ of an intermediate two-phase region of vesicles and elongated micelles in mixtures of tetradecyldimethylamine oxide $\cdot\frac{1}{2}\text{HCl}$ with Na^+NphS^- salt. This region separates a phase of elongated

micelles at low salt concentration from another of unilamellar vesicles at a higher salt concentration.

The contour of the titration curves in mixtures containing SDBS reflects the presence of aggregates and binding of histidine to the SDBS micelles-vesicles. The collapse of the data into one curve when the number of equivalents is less than 1 indicates that most of the histidine is free in solution, so the titration in these micellar solutions proceeds similarly to that of histidine in water. When the number of equivalents is greater than 1, the bounded histidine transforms the micelles into vesicles and the presence of histidine molecules on the surface of the vesicles gives rise to the slope deviations. Ionizable molecules on the surface of aggregates are known to change the apparent solution $\text{p}K_a$.⁴⁸ With more SDBS in solution, there are a higher number of aggregates and more histidine can bind; thus, a flatter slope is observed.

Vesicle formation in solutions with imidazole confirms that the amine and carboxyl groups in the amino acid are spectators for the micelle-to-vesicle transition. It is not surprising to observe this transition at a higher pH than in solutions with histidine, since a $\text{p}K_a$ of 7.0 of an imidazole molecule is higher than that of the imidazole group in histidine. In addition, binding of the imidazole molecules to SDBS is easier than binding of the imidazole group in histidine to SDBS, since the imidazole molecule is free of any steric hindrance caused by the amino acid backbone. However, once all of the imidazole molecules protonate, no more positive charges can be introduced into solution from decreasing pH, which explains why at least 15 mM imidazole has to be in solution in order to observe vesicles.

Conclusions

In mixtures of SDBS with histidine, a decrease in pH first elongates the micelles and then favors a micelle-to-vesicle transition with a region of coexistence of elongated micelles and vesicles. From CONTIN and SANS measurements, this transition appears to be continuous, so that the number of micelles decreases once the vesicles begin to form. Cryo-TEM confirms the presence of unilamellar vesicles. Binding of the positively charged imidazole group in the amino acid to the negatively charged benzenesulfonate headgroups allows for these morphological transitions. A similar transition is observed in mixtures of the imidazole molecule with SDBS. Vesicle formation depends mainly on the net charge of the imidazole-containing species, which is controlled by pH. With less histidine or imidazole in solution, the transition occurs at a lower pH because more of these molecules must protonate for the transition to occur.

Acknowledgment. We acknowledge the support of the National Science Foundation CTS-9814399 and CTS-0436195 and a NSF graduate fellowship to Y.I.G. The National Institute of Standards and Technology, U.S. Department of Commerce, provided the neutron scattering facilities used in this work, which were supported in part by the NSF under Agreement No. DMR-9986442.

References and Notes

- (1) van Nostrum, C. F. *Adv. Drug Delivery Rev.* **2004**, *56*, 9.
- (2) Liu, S. Y.; Weaver, J. V. M.; Save, M.; Armes, S. P. *Langmuir* **2002**, *18*, 8350.
- (3) Chilkoti, A.; Dreher, M. R.; Meyer, D. E. *Adv. Drug Delivery Rev.* **2002**, *54*, 1093.
- (4) Gradziński, M. *J. Phys.: Condens. Matter* **2003**, *15*, R655.
- (5) Tondre, C.; Caillet, C. *Adv. Colloid Interface Sci.* **2001**, *93*, 115.
- (6) Estroff, L. A.; Hamilton, A. D. *Chem. Rev.* **2004**, *104*, 1201.
- (7) Hamley, I. W. *Angew. Chem., Int. Ed.* **2003**, *42*, 1692.

- (8) Hentze, H. P.; Co, C. C.; McKelvey, C. A.; Kaler, E. W. *Colloid Chemistry I*; Topics in Current Chemistry 226; Springer-Verlag GmbH: Duesseldorf, Germany, 2003; p 197.
- (9) Liu, P.; Tian, J.; Liu, W. M.; Xue, Q. *J. Prog. Chem.* **2004**, *16*, 15.
- (10) Rao, G. C. S.; Kumar, M. S.; Mathivanan, N.; Rao, M. E. B. *Pharmazie* **2004**, *59*, 5.
- (11) Cevc, G. *Adv. Drug Delivery Rev.* **2004**, *56*, 675.
- (12) de Oliveira, A. G.; Scarpa, M. V.; Correa, M. A.; Cera, L. F. R.; Formariz, T. P. *Quim. Nova* **2004**, *27*, 131.
- (13) Li, X. J.; Schick, M. *Biophys. J.* **2001**, *80*, 1703.
- (14) Sommerdijk, N.; Lambermon, M. H. L.; Feiters, M. C.; Nolte, R. J. M.; Zwanenburg, B. *Chem. Commun.* **1997**, 455.
- (15) Bergsma, M.; Fielden, M. L.; Engberts, J. J. *Colloid Interface Sci.* **2001**, *243*, 491.
- (16) Johnsson, M.; Wagenaar, A.; Engberts, J. J. *Am. Chem. Soc.* **2003**, *125*, 757.
- (17) Franceschi, S.; de Viguerie, N.; Riviere, M.; Lattes, A. *New J. Chem.* **1999**, *23*, 447.
- (18) Wang, C. Z.; Gao, Q.; Huang, J. B. *Langmuir* **2003**, *19*, 3757.
- (19) Imae, T.; Hayashi, N.; Matsumoto, T.; Tada, T.; Furusaka, M. J. *Colloid Interface Sci.* **2000**, *225*, 285.
- (20) Nacka, F.; Cansell, M.; Gouygou, J. P.; Gerbeaud, C.; Meleard, P.; Entressangles, B. *Colloids Surf., B* **2001**, *20*, 257.
- (21) Edwards, K.; Silvander, M.; Karlsson, G. *Langmuir* **1995**, *11*, 2429.
- (22) Collins, D.; Litzinger, D. C.; Huang, L. *Biochim. Biophys. Acta* **1990**, *1025*, 234.
- (23) Kawasaki, H.; Souda, M.; Tanaka, S.; Nemoto, N.; Karlsson, G.; Almgren, M.; Maeda, H. *J. Phys. Chem. B* **2002**, *106*, 1524.
- (24) Kawasaki, H.; Imahayashi, R.; Tanaka, S.; Almgren, M.; Karlsson, G.; Maeda, H. *J. Phys. Chem. B* **2003**, *107*, 8661.
- (25) Kawasaki, H.; Imahayashi, R.; Maeda, H. *Langmuir* **2002**, *18*, 8358.
- (26) Gonzalez, Y. I.; Stjerdahl, M.; Danino, D.; Kaler, E. W. *Langmuir* **2004**, *20*, 7053.
- (27) The approximate distribution of benzenesulfonate isomers is the following: 4.4% C₁₀, 14.9% C₁₁, 66.0% C₁₂, 10.3% C₁₃, and 4.4% C₁₄. The isomers are 100% branched. The calculations were performed by summing the peak areas in the branched and linear regions of C₁₀–C₁₄ chromatograms which were obtained by the high performance liquid chromatography and mass spectrometry method. Smith, C.; Lynch, M. L. 2003, Procter & Gamble Co., Cincinnati, OH.
- (28) Koppel, D. E. *J. Chem. Phys.* **1972**, *57*, 4814.
- (29) Provencher, S. W. *Comput. Phys. Commun.* **1982**, *27*, 229.
- (30) Bellare, J. R.; Davis, H. T.; Scriven, L. E.; Talmon, Y. *J. Electron Microsc. Tech.* **1988**, *10*, 87.
- (31) Barker, J. G.; Pedersen, J. S. *J. Appl. Crystallogr.* **1995**, *28*, 105.
- (32) Bartlett, P.; Ottewill, R. H. *J. Chem. Phys.* **1992**, *96*, 3306.
- (33) Hansen, J. P.; Hayter, J. B. *Mol. Phys.* **1982**, *46*, 651.
- (34) Guinier, A.; Fournet, G. *Small-Angle Scattering of X-rays*; John Wiley and Sons: New York, 1955.
- (35) Kaler, E. W.; Herrington, K. L.; Murthy, A. K.; Zasadzinski, J. A. N. *J. Phys. Chem.* **1992**, *96*, 6698.
- (36) Chang, N. J.; Kaler, E. W. *J. Phys. Chem.* **1985**, *89*, 2996.
- (37) Liu, S. Y.; Gonzalez, Y. I.; Kaler, E. W. *Langmuir* **2003**, *19*, 10732.
- (38) Garrett, R. H.; Grisham, C. *Biochemistry*, 2nd ed.; Saunders College Publishing: Fort Worth, TX, 1999.
- (39) Israelachvili, J. *Intramolecular & Surface Forces*, 2nd ed.; Academic Press: London, 1991.
- (40) Soderman, O.; Herrington, K. L.; Kaler, E. W.; Miller, D. D. *Langmuir* **1997**, *13*, 5531.
- (41) Lin, Z. C.; Fu, Y. C. *J. Colloid Interface Sci.* **1996**, *184*, 325.
- (42) Sein, A.; Engberts, J. *Langmuir* **1995**, *11*, 455.
- (43) Hassan, P. A.; Raghavan, S. R.; Kaler, E. W. *Langmuir* **2002**, *18*, 2543.
- (44) Hassan, P. A.; Fritz, G.; Kaler, E. W. *J. Colloid Interface Sci.* **2003**, *257*, 154.
- (45) Edwards, K.; Almgren, M. *J. Colloid Interface Sci.* **1991**, *147*, 1.
- (46) Gustafsson, J.; Oradd, G.; Almgren, M. *Langmuir* **1997**, *13*, 6956.
- (47) Edwards, K.; Gustafsson, J.; Almgren, M.; Karlsson, G. *J. Colloid Interface Sci.* **1993**, *161*, 299.
- (48) Maeda, H.; Kakehashi, R. *Adv. Colloid Interface Sci.* **2000**, *88*, 275.